Topological Order and Criticality in (2+1)D Monitored Random Quantum Circuits

Ali Lavasani,[1,2] Yahya Alavirad,[1,2,3] and Maissam Barkeshli[1,2]
[1]Condensed Matter Theory Center, University of Maryland, College Park, Maryland 20742, USA
[2]Joint Quantum Institute, University of Maryland, College Park, Maryland 20742, USA
[3]Department of Physics, University of California at San Diego, La Jolla, California 92093, USA

(Received 5 January 2021; accepted 8 November 2021; published 1 December 2021)

It has recently been discovered that random quantum circuits provide an avenue to realize rich entanglement phase diagrams, which are hidden to standard expectation values of operators. Here we study $(2+1)$D random circuits with random Clifford unitary gates and measurements designed to stabilize trivial area law and topologically ordered phases. With competing single qubit Pauli-Z and toric code stabilizer measurements, in addition to random Clifford unitaries, we find a phase diagram involving a tricritical point that maps to $(2+1)$D percolation, a possibly stable critical phase, topologically ordered, trivial, and volume law phases, and lines of critical points separating them. With Pauli-Y single qubit measurements instead, we find an anisotropic self-dual tricritical point, with dynamical exponent $z \approx 1.46$, exhibiting logarithmic violation of the area law and an anomalous exponent for the topological entanglement entropy, which thus appears distinct from any known percolation fixed point. The phase diagram also hosts a measurement-induced volume law entangled phase in the absence of unitary dynamics.

DOI: 10.1103/PhysRevLett.127.235701

Introduction.—In the past few years, it has been realized that the interplay between measurements and unitary dynamics can give rise to rich physics in the dynamics of quantum entanglement [1–37]. Originally, it was shown that when $(1+1)$D random unitary dynamics are intercepted by local measurements at a rate p, the system can undergo a phase transition from a volume law entangled phase at $p < p_c$ to an area law entangled phase at $p > p_c$ [1–3]. Importantly, these phase transitions are entirely hidden from simple expectation values of operators but are manifest in *quantum-trajectory averaged* dynamics of entanglement measures, like the entanglement entropy (EE) [1,2,4,21].

Recently, it was shown that competing measurements can give rise to entanglement transitions even in the absence of unitary dynamics [21,22,28,34]. Furthermore, it was discovered that distinct $(1+1)$D area law phases can remain well defined in the context of random quantum circuits [21,22].

In this work, we consider a class of $(2+1)$D random quantum circuits that extrapolate between (i) a topologically ordered phase, characterized by nonzero topological entanglement entropy (TEE) [38,39] and realized by measuring the $\mathbb{Z}_2$ toric code stabilizers [40], (ii) a volume law entangled phase realized by random Clifford unitaries and, (iii) the trivial, area law phase realized by single-site measurements. As for the single-site measurements, we study both Pauli-Z and Pauli-Y measurements. This generalizes the work of Ref. [21] to $(2+1)$D where symmetry restrictions are not necessary. Similar to Ref. [21], at each step of the circuit, an element corresponding to one of the three phases is selected at random with probability p_g, p_u, p_s, respectively (subject to the condition $p_g + p_u + p_s = 1$).

Two typical arrangements of our circuits together with numerically calculated phase diagrams are shown in Fig. 1. We find stable topological, trivial area law, volume law (even without unitary dynamics), and critical phases. Notably, we also find evidence of several qualitatively distinct multicritical points.

In the absence of unitary dynamics and in the case where single qubits are only measured in the Pauli-Z basis, we find an exact analytical mapping between a 3D classical bond percolation problem and the dynamics of entanglement. We show that EE of rectangular regions are related to the number of clusters shared between that region and the rest of the system in percolation picture.

On the other hand, when single qubits are only measured in the Y direction, we show that an Ising duality restricts the phase diagram. We find a novel tricritical point at the self-dual point $(p_z, p_y) = (0, 0.5)$, separating topological, trivial area law, and volume law phases, in which the critical behavior of the system is qualitatively different from the rest of the phase diagram. Intriguingly, the circuit has nontrivial subsystem symmetries at this point.

Extensive numerical study of the phase diagram shows that *away* from the self-dual point discussed above: (i) The critical points are area law entangled, similar to usual $(2+1)$D scale invariant field theories. The subleading correction to this area-law scaling also agrees with results found in a variety of $(2+1)$D scale invariant field theories [41–44] (in contrast to the results of Ref. [30]). (ii) We find a correlation length exponent $\nu = 0.8(1)$ and a dynamical

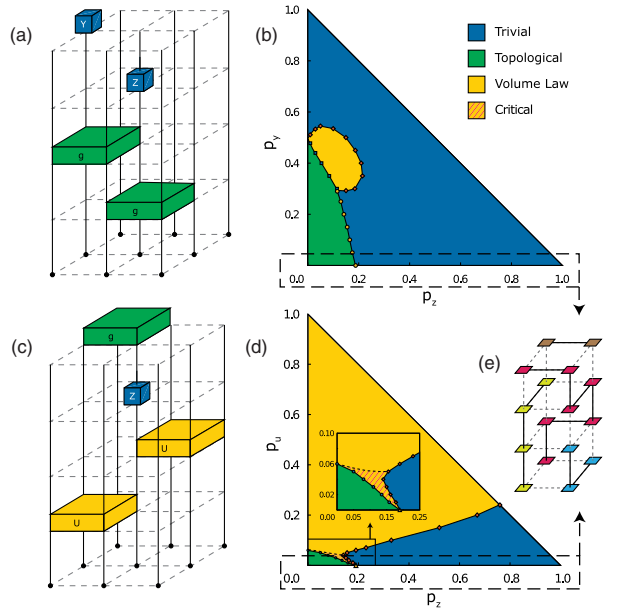

FIG. 1. (a) A typical measurement-only random circuit. (b) Phase diagram of $(2+1)$D measurement-only random circuits. (c) A typical hybrid random circuit. (d) Phase diagram of $(2+1)$D hybrid random circuits. (e) Entanglement dynamics at the $p_y = 0$ line of measurement-only random circuits (as well as the $p_u = 0$ line of hybrid random circuits) maps to a classical bond percolation problem on a cubic lattice.

critical exponent $z = 1$, which are set by the classical 3D bond percolation theory. Within margin of error, these exponents stay constant along phase boundaries.

However, the critical dynamics at the self-dual $p_z = 0$, $p_y = 0.5$ point is entirely distinct and characterized by (i) logarithmic corrections to the area law scaling of EE reminiscent of Fermi liquids, (ii) nonpercolation correlation length exponent $\nu = 0.47(8)$ and a dynamical critical exponent $z = 1.46(6)$, and (iii) a nonzero anomalous $\gamma = 1.0(2)$ exponent for the TEE [see Eq. (2)].

Models.—We consider $N = L^2$ qubits laid on the vertices of a two-dimensional periodic square lattice of linear length $L_x = L_y = L$. Three different sets of gates are considered where each gate set, when applied exclusively, drives the system into one of the distinct phases discussed above.

For the topological phase, we consider measurements corresponding to toric code stabilizers,

$$g_{i,j} = \begin{cases} X_{i,j}X_{i+1,j}X_{i,j+1}X_{i+1,j+1} & i+j \text{ is even} \\ Z_{i,j}Z_{i+1,j}Z_{i,j+1}Z_{i+1,j+1} & i+j \text{ is odd} \end{cases}, \quad (1)$$

where (i, j) denote the coordinates and $X_{i,j}$ and $Z_{i,j}$ are the Pauli operators acting on the corresponding qubit. We denote the set of all $g_{i,j}$ operators as $\mathcal{M}_g$.

For the trivial phase, we can pick any set of single qubit measurements. We use $\mathcal{M}_P$ to denote the set of single qubit Pauli-P operators (P could be either X, Y or Z). For the volume law phase, we use the set $\mathcal{C}_4$ consisting of four qubit Clifford unitaries $U_{i,j}$, acting on neighboring qubits located at (i, j), $(i+1, j)$, $(i, j+1)$, and $(i+1, j+1)$.

We study two types of random circuits. First, we consider measurement-only random circuits comprised of only measurements. More specifically, we start with the product state $|0\rangle^{\otimes N}$ and at each updating step, we measure an operator which is chosen uniformly at random from either $\mathcal{M}_Z$ with probability p_z, $\mathcal{M}_Y$ with probability p_y, or $\mathcal{M}_g$ with probability $p_g = 1 - p_z - p_y$. Each time step is defined as N consecutive updating steps. A typical example of such a circuit is shown in Fig. 1(a).

We also consider hybrid random circuits, which are comprised of unitary gates as well as measurements. We start with $|0\rangle^{\otimes N}$ and at each updating step we either apply a gate chosen uniformly at random from $\mathcal{C}_4$ with probability p_u or measure an operator chosen uniformly at random from $\mathcal{M}_Z$ or $\mathcal{M}_g$ with probabilities p_z and $p_g = 1 - p_u - p_z$, respectively.

Order parameters.—One can use TEE [38,39] denoted by S_{topo} to distinguish phases. S_{topo} equals 1 for the eigenstates of the toric code Hamiltonian while it is 0 for quantum states in the trivial phase. As for the volume law phase, the contribution which is proportional to the size of each region cancels out and one may expect S_{topo} to vanish in this phase as well. However, the $(1+1)$D results [4,35] suggest that the EE of a region has subextensive contributions [33,35] in the volume law phase, which results in a system-size dependent value for S_{topo}. Our numerical results support this scenario.

We also utilize the ancilla order parameter introduced in Refs. [5,6], which captures the transition in purification dynamics. It is defined using N_a ancilla qubits in addition to the system qubits, as follows. First a random local Clifford unitary circuit of depth $O(N)$ is applied to the entire set (system + ancilla) of qubits, which results in a maximally entangled stabilizer state of all qubits. Next, the system qubits are evolved under the random quantum circuit of interest for T time steps and then the EE of the set of all ancilla qubits, denoted by $S_a(T)$, is measured. In the $T \to \infty$ limit, the ancilla system will be entirely disentangled from the system. However, this purification dynamics happens with a rate which depends on the phase of the system. In the trivial area law phase, the ancilla qubits will be disentangled in constant time, independent of the system size. In the topological phase, although the bulk disentangles in constant time, the logical qubits remain entangled with the ancilla system until a time exponentially large in system size. In the volume law phase, the bulk remains entangled with the ancilla qubits up to exponentially large time steps. Therefore for large enough system sizes and at $T = \mathcal{O}(L)$, $S_a(T)$ will be 0, N_L and N_a in trivial, topological and volume law phases, respectively, where N_L denotes the number of logical qubits in the

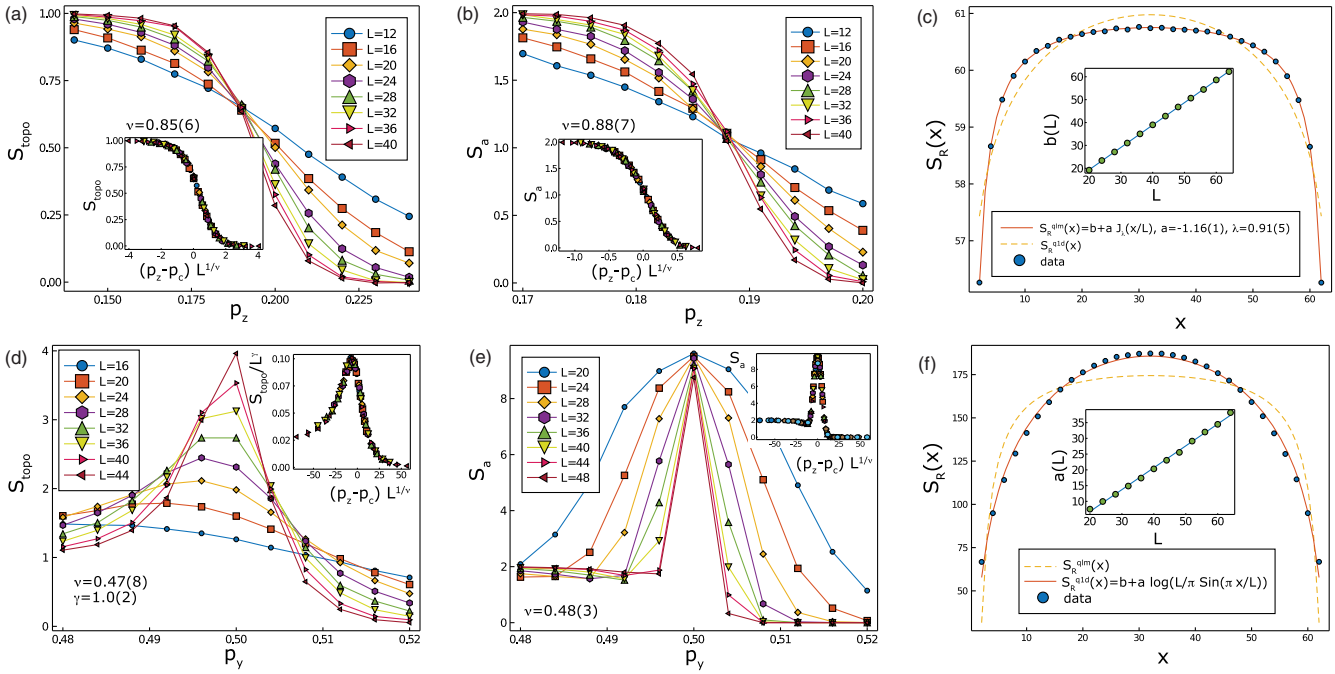

FIG. 2. Phase transitions across the $p_y = 0$ (top row) and $p_z = 0$ (bottom row) lines of the phase diagram for the measurement-only circuit: (a) S_{topo} and (b) S_a measured at $t = 4L$ versus p_z for fixed $p_y = 0$. Insets show the corresponding data collapse. (c) $S_R(x)$ for system size $L = 64$ at the percolation critical point $(p_z, p_y) = (0.188, 0)$, with the best fit of scaling functions $S^{\text{qlm}}(x)$ (solid line) and S^{q1D} (dashed line). The inset is the best fit value of the b parameter in Eq. (5) as a function of L. (d) S_{topo} and (e) S_a measured at $t = 0.6\,L^{1.46}$ versus p_y for fixed $p_z = 0$. Insets show the corresponding data collapse. (f) $S_R(x)$ for system size $L = 64$ at the self-dual critical point $(p_z, p_y) = (0, 0.5)$, with the best fit of scaling functions S^{q1D} (solid line) and $S^{\text{qlm}}(x)$ (dashed line). The inset shows the linear dependence of the best fit value of the a parameter in Eq. (4).

topological phase ($N_L = 2$ for the torus topology). We assumed that $N_L \ll N_a \ll L^2$. We use $N_a = 10$ ancillas throughout this work.

We note that while in our setting the purification transition occurs concurrently with TEE phase transition, they are not exactly the same [5]. One can, for instance, repeat the study here on a triangulation of a 2-sphere, for which $N_L = 0$, so purification protocols cannot distinguish the trivial and topological phases, while TEE can.

Results.—We start by studying the phase diagram of the measurement-only circuits. First, we focus on the $p_y = 0$ line. Notably, as shown in the Supplemental Material [45], there is an exact mapping which maps the entanglement dynamics at this line of the phase diagram to a classical bond percolation problem on a 3D cubic lattice. Figures 2(a) and 2(b) show the TEE and the ancilla order parameter as a function of p_z. As can be seen from the plots, there exists a stable topological phase extending up to $p_c \approx 0.2$, at which point a continuous phase transition takes the system to the trivial phase.

On general grounds, we may assume the following scaling forms governing the order parameters near the phase transition:

$$S_{\text{topo}}(p; L) = L^{\gamma} F[(p - p_c)L^{1/\nu}], \tag{2}$$

$$S_a(p, t, L) = G[(p - p_c)L^{1/\nu}, t/L^z], \tag{3}$$

where $F(x)$ and $G(x)$ are arbitrary functions and ν and z are the correlation length critical exponent and dynamical critical exponent, respectively. We find our data for the percolation critical point to be consistent with setting γ to 0. By collapsing S_{topo} near the critical point for different system sizes, we find $p_c = 0.188(2)$ and $\nu = 0.85(6)$. Note that ν is consistent with the values obtained from numerical simulation of classical percolation in three dimensions [46]. By investigating the time dependence of the ancilla order parameter S_a at $p = p_c$, we find it to be consistent with $z = 1$ (see Supplemental Material [45] for relevant plots). Collapsing S_a at $t = O(L)$ then yields $\nu = 0.88(7)$, in agreement with the value found via collapsing S_{topo}.

Another quantity of interest is the scaling form of the EE with subsystem size at the critical point. We consider the cylindrical region R with a smooth boundary, which has length x in one direction and goes all the way around the torus in the other direction. Let $S_R(x)$ denote its EE. Note that the boundary length $|\partial R|$ is $2L$, independent of x. As is discussed in the Supplemental Material [45], in the percolation picture this quantity is related to the number of clusters with shared support on region R and its complement.

For a conventional CFT in $(2+1)$D, the nonuniversal leading area-law term scales with $|\partial R| = 2L$. The subleading term for a cylindrical subregion is less well understood and several forms have been suggested, among which two are of particular interest. One is a quasi-$(1+1)$D scaling function, inspired by the exact form found in $(1+1)$D CFTs, which seems to decently capture EE scaling in certain $(2+1)$D gapless models [42]

$$S_R^{\mathrm{q1d}}(x) = b + a \log\left[\frac{L}{\pi}\sin\left(\frac{\pi x}{L}\right)\right], \tag{4}$$

where b contains the nonuniversal area law term. The other relevant scaling form was originally derived for the quantum Lifshitz model [43] but was found to describe the EE scaling in various other $(2+1)$D gapless models as well, including some $(2+1)$D CFTs [41].

$$S_R^{\mathrm{qlm}}(x) = b + aJ_\lambda(x/L), \tag{5}$$

$$J_\lambda(u) = \log\left(\frac{\theta_3(i\lambda u)\theta_3[i\lambda(1-u)]}{\eta(2iu)\eta[2i(1-u)]}\right), \tag{6}$$

where $\theta_3(z)$ and $\eta(z)$ are the Jacobi theta function and the Dedekind eta function, respectively (see Supplemental Material [45] for definitions). b contains the nonuniversal area-law contribution and λ is a model parameter, which we will use to find the best fit.

Figure 2(c) shows $S_R(x)$ for system size $L = 64$ at p_c alongside the best fit of the scaling functions. As can be seen from the graph, $S_R^{\mathrm{qlm}}(x)$ results in a good fit (solid line), while S_R^{q1D} cannot capture the scaling form. Moreover, we find that the best fit values of $a = -1.16(1)$ and $\lambda = 0.91(5)$ for S_R^{qlm} remain constant for different system sizes within the margin of error (see Supplemental Material [45]). As is shown in the inset, the b parameter scales linearly with system size, which shows that the leading term scales with $|\partial R|$.

We now turn our attention to the $p_z = 0$ line. Here the circuit has a self-duality mapping $p_y \to 1 - p_y$. Note that along this line, the system has $2L$ subsystem symmetries generated by the product of Y (or stabilizer) operators along horizontal or vertical loops, e.g., $\prod_j Y_{i,j}$. On a related note, there is a unitary transformation which maps the g and Y operators to the gauge operators of the $2D$ Bacon-Shor subsytem code [47,48] on a square lattice (see the Supplemental Material [45] for details).

By examining the TEE S_{topo} [Fig. 2(d)], we find the topological phase to be extended up to the self-dual point $p_y = 0.5$. However, at $p_y = 0.5$, S_{topo} grows with system size, which suggests a nonzero γ exponent. Collapsing S_{topo} data near the critical point yields $p_c = 0.502(1)$, $\gamma = 1.0(2)$, and $\nu = 0.47(8)$, which shows that this critical point is distinct from the percolation fixed point. Moreover, by looking at the time dependence of the ancilla order parameter at $p_y = 0.5$, we find that, in contrast to the percolation critical point, the best fit to the scaling form in Eq. (2) corresponds to $z = 1.46(8)$ (see Supplemental Material [45] for relevant plots). Accordingly, by collapsing $S_a(p, t, L)$ data at $t = O(L^{1.46})$ [Fig. 2(e)], we find $\nu = 0.48(3)$, in agreement with the result obtain from collapsing S_{topo}.

As for the cylindrical subregion EE $S_R(x)$ [Fig. 2(f)], we find that the quasi-1D scaling form $S^{\mathrm{q1d}}(x)$—rather than $S^{\mathrm{qlm}}(x)$—fits the data. However, as is shown in the inset, the a parameter in Eq. (5) is not constant, but has a linear dependence on system size L, demonstrating that the leading term scales as $L \log L$ rather than L as is expected in an area law state. The origin of the $L \log L$ violation is unclear; it may be related to the existence of subsystem symmetries along the $p_z = 0$ axis, which translates to the stabilizers of the Bacon-Shor code under the aforementioned duality map.

The rest of the phase diagram can be determined analogously [Fig. 1(a)]. We find that the percolation critical point is part of a critical line that persists up to some finite nonzero value of p_y, while the self-dual critical point at $(p_z, p_y) = (0, 0.5)$ splits into two critical lines with an intermediate volume law entangled phase in between, making it tricritical. Interestingly, the numerical data for all critical points that we considered, other than $(p_z, p_y) = (0, 0.5)$, are consistent with $z = 1$ and $\gamma = 0$, with ν remaining close to 0.8, similar to the percolation critical point. Their EE scaling is given by $S^{\mathrm{qlm}}(x)$ as well, with an area law scaling leading term. Remarkably, this makes the self-dual point special in this regard, as it is the only point in the phase diagram with $L \log L$ violation of area law, as well as quite different ν and γ exponents. We also note that the extracted a and λ parameters in $S^{\mathrm{qlm}}(x)$ change throughout the phase diagram. The relevant plots can be found in the Supplemental Material [45].

Lastly we present the numerical results for the hybrid random circuit which has unitary dynamics. The $p_u = 0$ line of phase diagram is exactly the same as $p_z = 0$ line of the measurement-only random circuit. Figure 3(a) shows

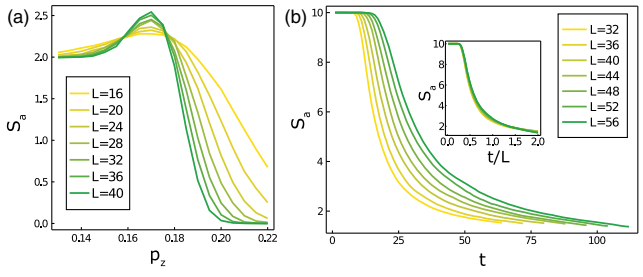

FIG. 3. (a) The ancilla EE S_a measured at $t = L$ as a function of p_z for fixed $p_u = 0.01$ in the hybrid random circuit. (b) S_a as a function of time at $(p_z, p_u) = (0.17, 0.01)$ in the hybrid random circuit. The inset is the same, plotted as a function of t/L.

the ancilla order parameter along $p_u = 0.01$, which signals the emergence of an intervening phase between topological and trivial phases, suggesting that the percolation critical point is actually a tricritical point in this phase diagram. In the intermediate phase, S_a does not saturate to $N_a = 10$, as is expected to be the case in the volume law phase, but rather increases weakly with system size, showing indications that it may saturate at a finite value less than 10. Indeed, for a point in the intermediate phase and for large systems, $S_a(t; L)$ seems to be a function of only t/L [Fig. 3(b)] which is a signature of a critical phase with $z = 1$ [see Eq. (3)]. Moreover, we find that in the intermediate phase, $S^{\mathrm{qlm}}(x)$ fits the EE of a cylindrical subregion as well. These points suggest that the intermediate phase is a critical region. Nonetheless, we remark that the observed behavior could be just related to finite size effects and the proximity to the critical lines.

The critical region extends to the p_u axis, ending at $p_u \approx 0.06$, which appears to be a tricritical point, although within the precision of this study, we cannot rule out the existence of a narrow critical region around $p_u = 0.06$. By collapsing the S_a data along the p_u axis, we find $p_c = 0.059(1)$ with critical exponent $\nu = 0.78(8)$. On the right, the critical region ends on the boundary of the trivial phase and the volume law phase. The trivial phase itself ends at $p_u = 0.238(2)$ along the $p_u + p_z = 1$ line. We find $\nu = 0.80(7)$ at the corresponding phase transition (see the Supplemental Material [45] for relevant plots). The overall phase diagram of the hybrid circuit in two dimensions is illustrated in Fig. 1(b).

We thank David Huse and Michael Gullans for discussions. The authors acknowledge the University of Maryland supercomputing resources made available for conducting the research reported in this Letter. A. L. and M. B. are supported by NSF CAREER (DMR-1753240) and Alfred P. Sloan Research Fellowship. Y. A. is supported by the Simons Collaboration on Ultra-Quantum Matter, Grant No. 651440 from the Simons Foundation as well as University of California Laboratory Fees Research Program, Grant No. LFR-20-653926.

[1] B. Skinner, J. Ruhman, and A. Nahum, Phys. Rev. X **9**, 031009 (2019).
[2] Y. Li, X. Chen, and M. P. A. Fisher, Phys. Rev. B **98**, 205136 (2018).
[3] A. Chan, R. M. Nandkishore, M. Pretko, and G. Smith, Phys. Rev. B **99**, 224307 (2019).
[4] Y. Li, X. Chen, and M. P. A. Fisher, Phys. Rev. B **100**, 134306 (2019).
[5] M. J. Gullans and D. A. Huse, Phys. Rev. X **10**, 041020 (2020).
[6] M. J. Gullans and D. A. Huse, Phys. Rev. Lett. **125**, 070606 (2020).
[7] R. Vasseur, A. C. Potter, Y.-Z. You, and A. W. W. Ludwig, Phys. Rev. B **100**, 134203 (2019).
[8] S. Choi, Y. Bao, X.-L. Qi, and E. Altman, Phys. Rev. Lett. **125**, 030505 (2020).
[9] M. Szyniszewski, A. Romito, and H. Schomerus, Phys. Rev. B **100**, 064204 (2019).
[10] Q. Tang and W. Zhu, Phys. Rev. Research **2**, 013022 (2020).
[11] C.-M. Jian, Y.-Z. You, R. Vasseur, and A. W. W. Ludwig, Phys. Rev. B **101**, 104302 (2020).
[12] X. Cao, A. Tilloy, and A. D. Luca, SciPost Phys. **7**, 24 (2019).
[13] J. Lopez-Piqueres, B. Ware, and R. Vasseur, Phys. Rev. B **102**, 064202 (2020).
[14] Y. Bao, S. Choi, and E. Altman, Phys. Rev. B **101**, 104301 (2020).
[15] L. Piroli, C. Sünderhauf, and X.-L. Qi, J. High Energy Phys. 04 (2020) 063.
[16] A. Zabalo, M. J. Gullans, J. H. Wilson, S. Gopalakrishnan, D. A. Huse, and J. H. Pixley, Phys. Rev. B **101**, 060301(R) (2020).
[17] D. Rossini and E. Vicari, Phys. Rev. B **102**, 035119 (2020).
[18] J. Iaconis, A. Lucas, and X. Chen, Phys. Rev. B **102**, 224311 (2020).
[19] Y. Fuji and Y. Ashida, Phys. Rev. B **102**, 054302 (2020).
[20] N. Lang and H. P. Büchler, Phys. Rev. B **102**, 094204 (2020).
[21] A. Lavasani, Y. Alavirad, and M. Barkeshli, Nat. Phys. **17**, 342 (2021).
[22] S. Sang and T. H. Hsieh, Phys. Rev. Research **3**, 023200 (2021).
[23] X. Chen, Y. Li, M. P. A. Fisher, and A. Lucas, Phys. Rev. Research **2**, 033017 (2020).
[24] A. Nahum, S. Roy, B. Skinner, and J. Ruhman, PRX Quantum **2**, 010352 (2021).
[25] O. Lunt and A. Pal, Phys. Rev. Research **2**, 043072 (2020).
[26] M. Szyniszewski, A. Romito, and H. Schomerus, Phys. Rev. Lett. **125**, 210602 (2020).
[27] M. J. Gullans, S. Krastanov, D. A. Huse, L. Jiang, and S. T. Flammia, Phys. Rev. X **11**, 031066 (2021).
[28] A. Nahum and B. Skinner, Phys. Rev. Research **2**, 023288 (2020).
[29] O. Alberton, M. Buchhold, and S. Diehl, Phys. Rev. Lett. **126**, 170602 (2021).
[30] X. Turkeshi, R. Fazio, and M. Dalmonte, Phys. Rev. B **102**, 014315 (2020).
[31] L. Fidkowski, J. Haah, and M. B. Hastings, Quantum **5**, 382 (2021).
[32] S. Vijay, arXiv:2005.03052.
[33] R. Fan, S. Vijay, A. Vishwanath, and Y.-Z. You, Phys. Rev. B **103**, 174309 (2021).
[34] M. Ippoliti, M. J. Gullans, S. Gopalakrishnan, D. A. Huse, and V. Khemani, Phys. Rev. X **11**, 011030 (2021).
[35] Y. Li and M. P. A. Fisher, Phys. Rev. B **103**, 104306 (2021).
[36] M. Van Regemortel, Z.-P. Cian, A. Seif, H. Dehghani, and M. Hafezi, Phys. Rev. Lett. **126**, 123604 (2021).
[37] O. Shtanko, Y. A. Kharkov, L. P. Garcí-Pintos, and A. V. Gorshkov, arXiv:2004.06736.
[38] A. Kitaev and J. Preskill, Phys. Rev. Lett. **96**, 110404 (2006).
[39] M. Levin and X.-G. Wen, Phys. Rev. Lett. **96**, 110405 (2006).
[40] A. Kitaev, Ann. Phys. (Amsterdam) **303**, 2 (2003).

[41] X. Chen, G. Y. Cho, T. Faulkner, and E. Fradkin, J. Stat. Mech. 02 (2015) P02010.
[42] H. Ju, A. B. Kallin, P. Fendley, M. B. Hastings, and R. G. Melko, Phys. Rev. B **85**, 165121 (2012).
[43] J.-M. Stephan, H. Ju, P. Fendley, and R. G. Melko, New J. Phys. **15**, 015004 (2013).
[44] A. B. Kallin, E. Stoudenmire, P. Fendley, R. R. Singh, and R. G. Melko, J. Stat. Mech. 06 (2014) P06009.
[45] See Supplemental Material at http://link.aps.org/supplemental/10.1103/PhysRevLett.127.235701 for additional plots and details about the percolation mapping, the duality mappings and error estimates.
[46] J. Wang, Z. Zhou, W. Zhang, T. M. Garoni, and Y. Deng, Phys. Rev. E **87**, 052107 (2013).
[47] D. Bacon, Phys. Rev. A **73**, 012340 (2006).
[48] P. W. Shor, Phys. Rev. A **52**, R2493 (1995).